Journal of
MATERIALS RESEARCH

Growth and electronic properties of epitaxial TiN thin films on 3C-SiC(001) and 6H-SiC(0001) substrates by reactive magnetron sputtering

L. Hultman, H. Ljungcrantz, C. Hallin, E. Janzén, and J-E. Sundgren
Department of Physics, Linköping University, S-581 83 Linköping, Sweden

B. Pécz
Research Institute for Technical Physics of the Hungarian Academy of Sciences, H-1325 Budapest, P.O. Box 76, Hungary

L. R. Wallenberg
Inorganic Chemistry 2, Chemical Center, Lund University, P.O. Box 124, S-221 00 Lund, Sweden

(Received 18 December 1995; accepted 22 April 1996)

Epitaxial TiN films were grown on cubic (3C)-SiC(001) and hexagonal (6H)-SiC(0001) substrates by ultrahigh vacuum reactive magnetron sputtering from a Ti target in a mixed Ar and N_2 discharge at a substrate temperature of 700 °C. Cross-sectional transmission electron microscopy, including high-resolution imaging, showed orientational relationships TiN(001) ‖ 3C-SiC(001), and TiN[110] ‖ 3C-SiC[110], and TiN(111) ‖ 6H-SiC(0001) and TiN[110],[101] ‖ 6H-SiC[$1\bar{2}10$]. In the latter case, twin-related TiN domains formed as the result of nucleation on SiC terraces with an inequivalent stacking sequence of Si and C. The TiN/SiC interface was locally atomically sharp for both SiC polytypes. Defects in the TiN layers consisted of threading double positioning domain boundaries in TiN(111) on 6H-SiC. Stacking faults in 3C-SiC did not propagate upon growth of TiN. Room-temperature resistivity of TiN films was $\rho = 14\ \mu\Omega$ cm for 6H-SiC(0001) and $\rho = 17\ \mu\Omega$ cm for 3C-SiC(001) substrates. Specific contact resistance of TiN to 6H-SiC(0001) was $1.3 \times 10^{-3}\ \Omega\ \text{cm}^2$ for a 6H-SiC substrate with an *n*-type doping of $5 \times 10^{17}\ \text{cm}^{-3}$.

I. INTRODUCTION

Wide band gap SiC's of hexagonal (6H) and cubic (3C) polytypes are currently being implemented in high-temperature and high-power electronic devices. For both applications, stable contact layers are needed. While several metals have been applied as contacts to SiC, interfacial stability is limiting the contact performance at elevated temperatures.[1–8] For example, Co thin films on α–SiC exhibit interfacial reaction during annealing at 800–1000 °C.[2,3] The lowest observed specific contact resistance values ($\sim 1 \times 10^{-6}\ \Omega\ \text{cm}^2$) are from Ni contacts deposited on *n*-type epitaxial SiC layer doped to more than $1 \times 10^{19}\ \text{cm}^{-3}$ and annealed at 1000 °C.[9]

Titanium nitride has been proposed as a contact material to SiC, and polycrystalline TiN layers on 6H-SiC were shown to exhibit ohmic behavior.[5] However, the nitrogen ion irradiation applied to the substrates prior to TiN deposition by ion-assisted reactive evaporation yielded an amorphous region at the TiN/SiC interface.[5] The effectiveness of TiN as a contact material is due to its low resistivity (15–100 $\mu\Omega$ cm depending on the crystalline perfection[10]) and high thermal stability.[11] While epitaxial growth of TiN films has been reported for a number of electronic substrate materials including Si(001)[12,13] and GaAs(110),[14] there are, to our knowledge, no reports of the single-crystal TiN/SiC system.

II. EXPERIMENTAL DETAILS

TiN films were deposited to a thickness of 0.2 μm in a dc planar magnetron sputtering system equipped with a 1000 $1\ \text{s}^{-1}$ turbo-molecular pump. The background pressure of the system was 1.4×10^{-7} Pa (1×10^{-9} Torr) and with the substrate heater operating $\leq 7 \times 10^{-7}$ Pa (5×10^{-9} Torr). The circular (7.5 cm in diameter) water-cooled Ti target (purity 99.9%) was positioned 13 cm under the substrate holder. The depositions were carried out in mixed discharge with equal amounts of Ar (purity 99.9997%) and N_2 (purity 99.9999%) and a total pressure of 2 mTorr monitored with a capacitance nanometer. A constant power supply was used to keep the target power at 0.5 kW, which resulted in a target voltage of 435 V and a current of 1.15 A. These conditions resulted in a deposition rate of $0.12\ \text{nm}\,\text{s}^{-1}$. The substrate table was kept at a floating potential that was measured to be −10 V.

The substrates were on-axis 6H-SiC(0001) wafers (CREE Research, Inc.), Si-face polished, and *n*-type (doping level 5×10^{17} cm^{-3}) and 3C-SiC(001) layers which were epitaxially grown by chemical vapor deposition on Si(100) substrates at a temperature of 1250 °C.[15] The growth process of 3C-SiC took place in a hot-wall type reactor using the silane-propane-hydrogen system.[16,17] The film quality of the 3C-SiC(001) layer was determined using x-ray diffraction which showed a full width at half maximum value of the SiC(001) peak as low as 0.075° 2θ.[15]

The substrates were ultrasonically cleaned in ethanol, dipped in HF, rinsed in distilled water, and dried in dry N_2 immediately prior to insertion into a load-lock system and then transferred into the deposition chamber. Before starting the depositions, the substrates were thermally degassed at 800 °C for 1 h after which the temperature was adjusted to the deposition temperature of 700 °C. Substrate temperature was measured with an infrared pyrometer using an emissivity factor of 0.8. A deposition sequence consisted of first adjusting the Ar and N_2 gas flows, sputter-cleaning the target for 10 min with a shutter covering the substrates, and then removing the shutter for depositing a TiN film to a thickness of 40–200 nm.

For sputter deposition, stoichiometric single-crystal TiN can also be obtained in more concentrated nitrogen discharges (including pure N_2) with deposition temperatures up to at least 850 °C.[17] For T_s decreasing below 700 °C, the film stoichiometry becomes increasingly more sensitive to the N_2 partial pressure, while epitaxial growth can be maintained to ~500 °C.

Samples for cross-sectional transmission electron microscopy (XTEM) were prepared by gluing two samples film-to-film, mounting them in a Ti grid, and mechanically grinding them to a thickness of ~50 μm. Thinning to electron transparency was accomplished in a Technoorg-Linda IV3 unit using Ar^+ ion milling with ion energies initially at 10 keV and then reduced to 3 keV. The beam was incident at a near grazing incidence of 3°. During final etching, the samples were continuously rocked ±40° about the normal of the film surface. TEM analysis was performed in JEOL 4000 EX and Philips CM 20 UT microscopes with point resolutions 1.6 Å and 1.9 Å, respectively, under imaging conditions close to the Scherzer focus.

The surface structures of the substrate and film were studied *in situ* by reflection high energy electron diffraction (RHEED) at 35 kV. The RHEED patterns were recorded with a CCD camera.

A colinear four-point probe,[18] with probe spacing 0.65 mm, was used to measure the resistivity, ρ, in the TiN films. To measure the specific contact resistance, ρ_c, the modified four-point configuration according to Kuphal[19] was adopted. The specific contact resistance can be calculated using the following equation:

$$\rho_c = \frac{A}{I_{ad}}\left[U_{ab} - R_s \times I_{ad} - U_{bc}\frac{\ln\left(3\frac{s}{d} - \frac{1}{2}\right)}{2\ln 2}\right], \quad (1)$$

where A is the contact area, I_{ad} is the current applied between contacts *a* and *d*, and U_{ab} and U_{bc} are the voltages measured between points *a*-*b* and *b*-*c*, respectively. R_s is the spreading resistance under the contact, *s* the spacing between contact points, and *d* the contact diameter. The four equidistant contacts (spacing 5 mm) was made by first evaporating four thick aluminum spots (200 μm diameter) through a shadow mask on the TiN film. The uncovered TiN was then etched away with a solution consisting of $NH_3 : H_2O_2 : H_2O$ (1 : 1 : 2).

III. RESULTS AND DISCUSSION

Figure 1 shows RHEED patterns of (a) 3C-SiC(001) and (b) 6H-SiC(0001) substrate surfaces obtained prior to deposition. 3C-SiC(001) showed a mixed 1×1 streak and bulk spot pattern caused by a small surface roughness in agreement with XTEM observations of 3C-SiC grown on Si(001) under similar conditions.[15] 6H-SiC(0001) exhibited a streaky 1×1 pattern with only a diffuse bulk spot pattern, indicating a relatively flat surface. The RHEED patterns of the corresponding TiN films obtained after termination of growth were streaky for the (001) orientation [see Fig. 1(c)] and streaky with diffuse intensity at the bulk spot positions for the (111) orientation [see Fig. 1(d)], both in alignment with the corresponding SiC lateral crystallographic directions.

Cross-sectional TEM was used for studying microstructural evolution and growth mode of the TiN layers. TiN layers on SiC substrates exhibited a homogeneous coverage as can be seen in Fig. 2 for (a) 3C-SiC(001) substrate and (b) 6H-SiC(0001) substrate. The TiN(001) film was homogeneous and exhibited a relatively flat top surface [see Fig. 2(a)]. Figure 2(b) shows for the TiN(111) case that the TiN layer exhibited twin-related TiN domains as described below with domain boundaries extending from the film-substrate interface to the film surface [marked by arrowheads in Fig. 2(b)]. The domains were 10–40 nm in width and exhibited a top surface with flat terraces interrupted by surface cusps and faceting at the domain boundaries as can be seen in the higher-magnification image of the TiN(111) top surface in Fig. 2(c).

High-resolution imaging and selected-area electron diffraction (SAD) showed that the TiN(111) film contained double-positioning domain boundaries (DPB) from the difference in stacking sequence of TiN islands nucleated on terraces on the 6H-SiC surface (marked by arrowheads in Fig. 3). Twin-related TiN

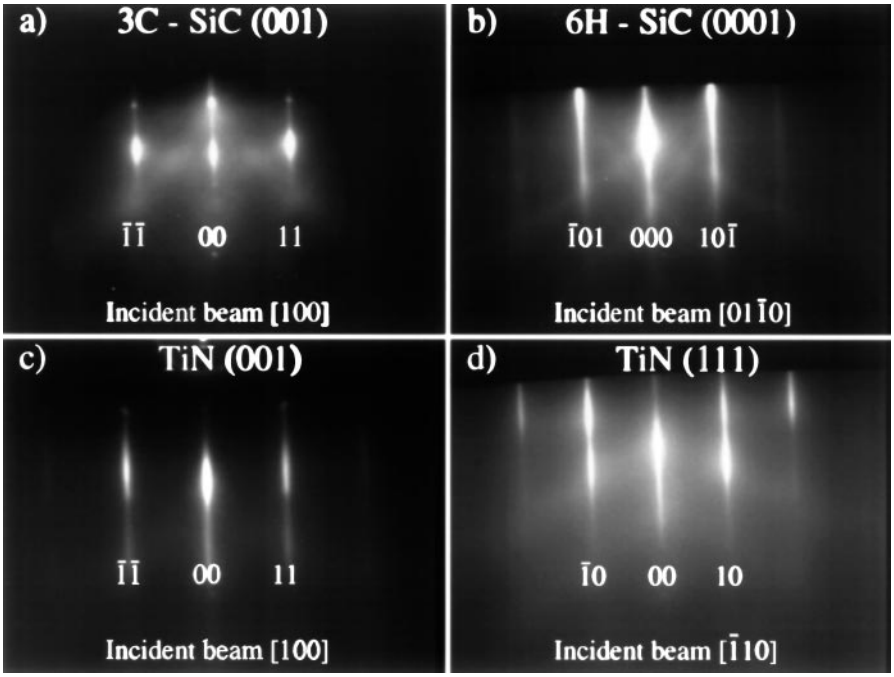

FIG. 1. Reflection high energy electron diffraction patterns obtained *in situ* in the deposition system of the (a) 3C-SiC(001) substrate and (b) 6H-SiC(0001) substrate, (c) TiN(001) film on SiC(001), and (d) TiN(111) film on SiC(0001).

domains representing ⟨110⟩ and ⟨101⟩ zone axes with common (111) planes, called hereafter A and B, were identified from SAD patterns and marked in Fig. 3. The domains were separated by incoherent twin boundaries. Superpositioning of the domains in the XTEM foil gives rise to double diffraction as evidenced by the SAD pattern inset (labelled A+B) and the presence of Moiré fringes in the lattice image with a spacing of three (111) lattice fringes. The orientational relationship was TiN($1\bar{1}1$) ‖ 6H-SiC(0001); TiN[110], [101](twins) ‖ 6H-SiC[$1\bar{2}10$]. Furthermore, at SiC terraces, the TiN/SiC interface was locally atomically sharp, as can be seen in the right portion of Fig. 3.

The steps separating the terraces at the TiN/6H-SiC interface were in fractions of the 6H-SiC unit cell (six Si–C bilayers, ~15 Å) as can be seen in Fig. 3. Previous scanning tunneling microscopy (STM) studies of identical on-axis 6H-SiC substrates have shown an irregular surface step distribution resulting from polishing-induced damage.[20] Also, the low-temperature substrate cleaning process employed here for the 6H-SiC(0001) resulted in a 1×1 reconstruction [see Fig. 1(b)]. In Ref. 20 this was associated with a remaining oxygen contamination corresponding to a coverage of ~1 monolayer. High-temperature surface preparation, however, results in $\sqrt{3} \times \sqrt{3}$ reconstruction and larger terraces of 6H-SiC separated by steps in multiples of three Si–C bilayers.[21] An improved SiC surface preparation should yield more flat TiN overlayers, and for the case of clean 6H-SiC(0001) with terraces separated by steps of unit cell height also suppress nucleation of twin-oriented TiN domains.

In the TiN(001)/3C-SiC(001) case, SiC surface roughness was dominated by nm-size steps and cusps at antiphase domain (APD) boundaries emerging at the surface. The APD's were the result of noncorrelated SiC nucleation on Si(001).[15]

In the case of TiN on 3C-SiC(001), Fig. 4 shows the orientational relationship TiN(001) ‖ 3C-SiC(001); TiN[110] ‖ 3C-SiC[110]. 3C-SiC film and Si substrate, in turn, exhibited the same relationship. TiN/3C-SiC interface was atomically sharp and contained misfit dislocations as marked in Fig. 4(a). Figure 4(b) shows the typical observation that stacking faults in the SiC did not propagate into the TiN. This is to be expected considering the extremely low stacking fault energy in SiC and that faults on TiN(111) are difficult to form. Stacking faults form in the 3C-SiC layer during nucleation on the Si(001) surface, but the fault density decreases with increasing film thickness due to the termination of intersecting faults.[15,22]

In the TiN/SiC epitaxial system, the nominal lattice mismatch of 3.2% was relieved at the interface by misfit dislocations. For TiN of 3C-SiC(001), the dislocations were extra half planes on TiN{111} planes [see Fig. 4(a)]. These, however, were not paired at the interface to form the more efficient strain-relieving misfit dislocations of the edge type with line direction [110] and Burgers vectors $1/2[1\bar{1}0]$ within the plane of the interface as expected for relaxed TiN layers.[23]

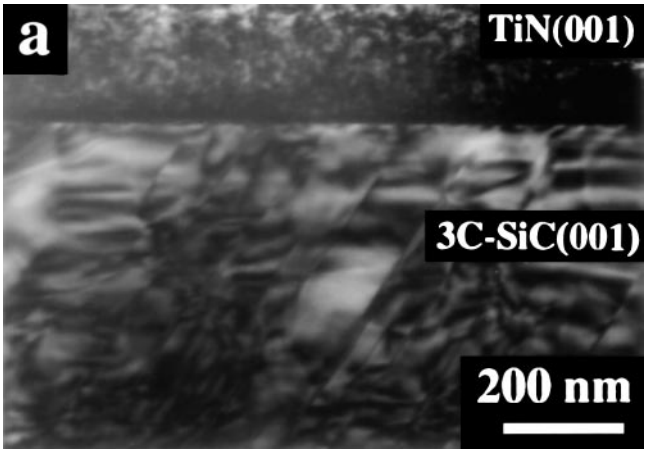

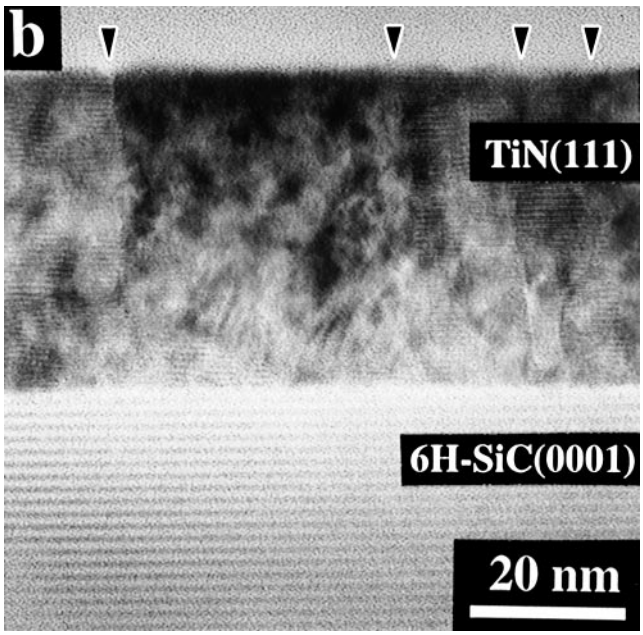

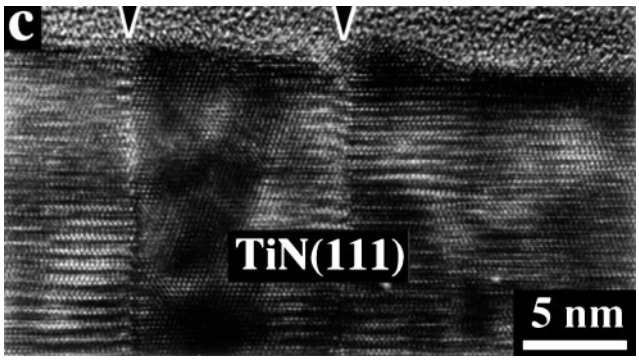

FIG. 2. Cross-sectional transmission electron micrographs from (a) TiN(001) film on the 3C-SiC(001) substrate, (b) TiN(111) film on the 6H-SiC(0001) substrate, and (c) high-resolution image of the TiN(111) top surface. TiN domain boundaries are marked by arrowheads in (b) and (c).

Room temperature resistivities, ρ, of 200-nm-thick as-deposited TiN(111) and TiN(001) films were found to be 14.2 ± 0.2 $\mu\Omega$ cm and $16.8 \pm$ $\mu\Omega$ cm, respectively.

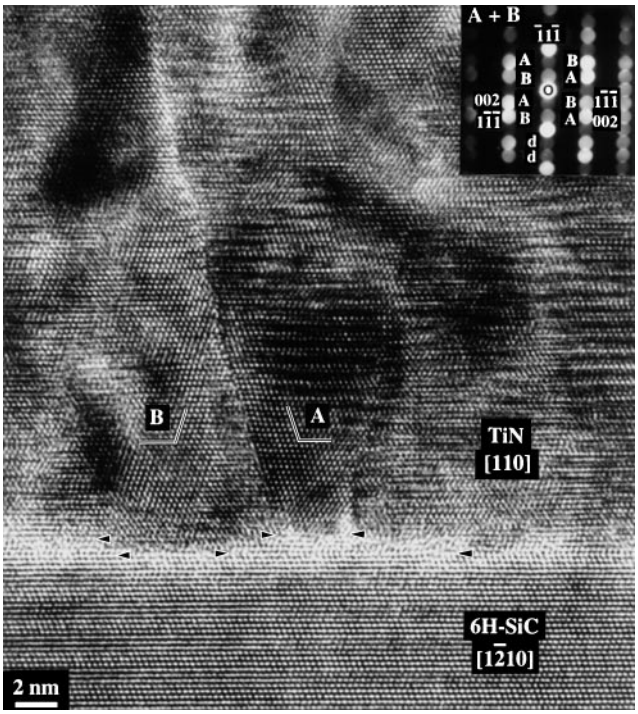

FIG. 3. Cross-sectional high-resolution image and selected-area electron diffraction (SAD) pattern from a TiN(111) film on the 6H-SiC(0001) substrate (SiC surface steps indicated by horizontal arrowheads) in the [1$\bar{2}$10] zone axis projection showing. Twin-related ($\bar{1}11$)-oriented TiN domains projected along $\langle 110 \rangle$ and $\langle 101 \rangle$ zone axes, respectively, are marked *A* and *B* in the image and *A* + *B* in the SAD pattern. Traces of {111} planes in domains *A* and *B* are marked by solid lines. Double diffraction in the SAD is marked *d.*

These resistivity values for TiN are somewhat lower than those previously reported for single-crystal TiN films grown on MgO substrates; $\rho^{(111)} = 15 \pm 3$ $\mu\Omega$ cm[10] and $\rho^{(001)} = 24$ $\mu\Omega$ cm.[24]

The specific contact resistance for TiN on 6H-SiC(0001) was $\rho_c = 1.3 \times 10^{-3}$ Ω cm^2. It should be noticed that the 6H-SiC substrate was low doped (5×10^{17} cm^{-3}), so ρ_c can be reduced further one or two orders of magnitude when using highly doped epitaxial SiC layers. The epitaxial TiN/SiC contact thus offers a promising candidate for a high-temperature ohmic contact. Single-crystal TiN should be preferred to polycrystalline TiN contacts by virtue of its lower resistivity.

As for the temperature stability of the TiN/SiC interface structure, initial cross-sectional TEM results from samples after rapid thermal annealing (3 °C s^{-1}) show that the structure is stable up to 1100 °C. Finally, we note that the deposition temperature (~700 °C) required for growth of μm-thick epitaxial TiN layers is compatible with SiC processing.

IV. CONCLUSIONS

Epitaxial TiN layers with sharp interfaces to the common polytypes of SiC can be obtained by reactive

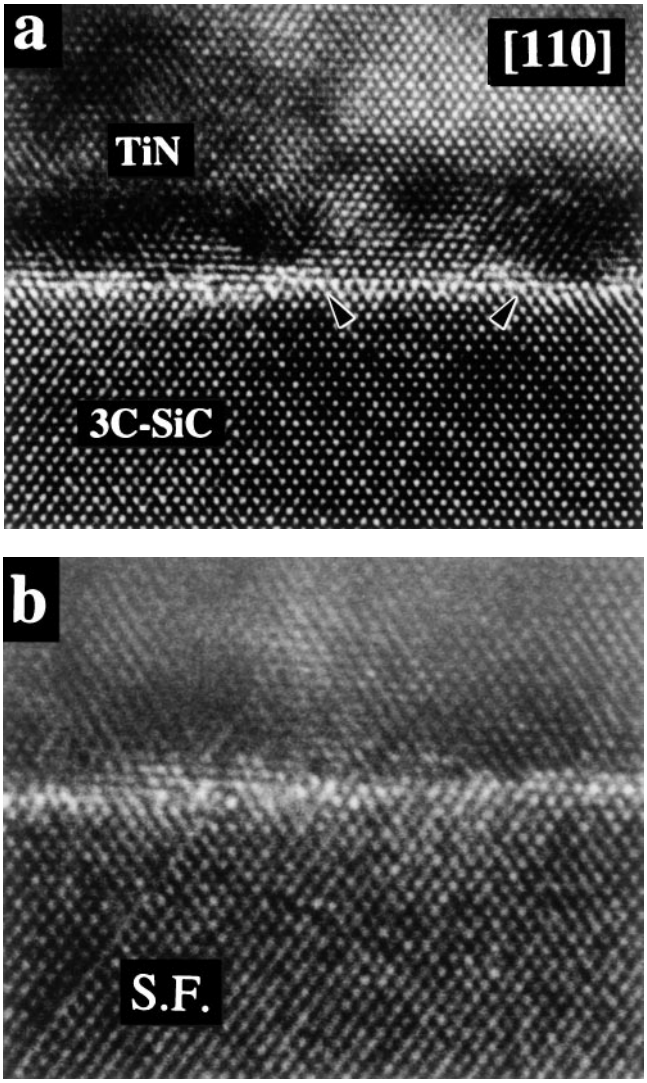

FIG. 4. Cross-sectional high-resolution images from a TiN(001) film on 3C-SiC(001) substrate layer in the [110] zone axis projection showing (a) an atomically sharp TiN/SiC interface with misfit dislocations (marked by arrowheads) and (b) a stacking fault in SiC (marked S.F.) terminating at the TiN film.

magnetron sputter deposition of TiN at 700 °C. The room-temperature resistivity of the as-grown TiN films was as low as 14 $\mu\Omega$ cm, and the specific contact resistance of TiN to 6H-SiC(0001) was 1.3×10^{-3} Ω cm^2 for a substrate doping of 5×10^{17} cm^{-3}. The TiN layer thus forms nonreactive contacts to SiC stable at least up to 700 °C.

ACKNOWLEDGMENTS

This work was supported by the Swedish Natural Research Council (NFR) and the Swedish Board for Technical Development (NUTEK)/NFR Material Consortium on Thin Film Growth. We acknowledge the collaboration with the Department of Materials, University of Oxford and the support from the European Commission through the Copernicus project CP 940603. Two of the authors, L. H. and L. R. W., acknowledge additional support from NFR. Dr. J. R. A. Carlsson and Ms. C. Engström are acknowledged for assistance with rapid thermal annealing experiment.

REFERENCES

1. J. Crofton, P. A. Barnes, J. R. Williams, and J. A. Edmond, Appl. Phys. Lett. **62**, 384 (1993).
2. N. Lundberg and M. Östling, Appl. Phys. Lett. **63**, 3069 (1993).
3. L. M. Porter, R. F. Davis, J. S. Bow, M. J. Kim, and R. W. Carpenter, J. Mater. Res. **10**, 26 (1995).
4. M. G. Rastegaeva and A. L. Syrkin, Sensors and Actuators A **33**, 95 (1992).
5. R. C. Glass, L. M. Spellman, S. Tanaka, and R. F. Davis, J. Vac. Sci. Technol. A **10**, 1625 (1992).
6. K. L. Moazed, Metall. Trans. A **23A**, 1999 (1992).
7. T. M. Parrill and Y. W. Chung, Surf. Sci. **271**, 395 (1992).
8. J. S. Chen, E. Kowala, M-A. Nicolet, L. Baud, C. Jaussaud, R. Madrar, and C. Bernard, J. Appl. Phys. **75**, 897 (1994).
9. C. Arnado, S. Tyc, F. Wyczinsk, and C. Brylisnki, Proc. ISCMRM 1995 (in press).
10. B-O. Johansson, J-E. Sundgren, J. E. Greene, A. Rockett, and S. A. Barnett, J. Vac. Sci. Technol. A **3**, 303 (1985).
11. C. Y. Ting and M. Wittmer, Thin Solid Films **96**, 327 (1982).
12. L. Hultman, C-H. Choi, W-A. Chiou, and S. A. Barnett, J. Vac. Sci. Technol. B **9**, 221 (1991).
13. J. Narayan, P. Tiwari, X. Chen, J. Singh, R. Chowdhury, and T. Zheleva, Appl. Phys. Lett. **61**, 12909 (1992).
14. T. Zheleva, K. Jagannadham, and J. Narayan, J. Appl. Phys. **75**, 860 (1994).
15. O. Kordina, L-O. Björketun, A. Henry, C. Hallin, R. C. Glass, L. Hultman, J-E. Sundgren, and E. Janzén, J. Cryst. Growth **154**, 303 (1995).
16. O. Kordina, C. Hallin, R. C. Glass, A. Henry, and E. Janzén, Proc. 5th Int. Conf. on Silicon Carbide and Related Materials (ICSCRM), Inst. of Phys. Conf. Series **137**, 41–44 (1993).
17. L. Hultman, S. A. Barnett, J-E. Sundgren, and J. E. Greene, J. Cryst. Growth **92**, 639 (1988).
18. D. K. Schroeder, in *Semiconductor Material and Device Characterization* (John Wiley & Sons, Inc., New York, 1990).
19. E. Kuphal, Solid State Electron. **24**, 69 (1981).
20. F. Owman, C. Hallin, P. Mårtensson, and E. Janzén, J. Cryst. Growth (in press).
21. F. Owman, C. Hallin, and P. Mårtensson, Surf. Sci. **330**, L639 (1995), and references therein.
22. Q. Wahab, M. R. Sardela, Jr., L. Hultman, A. Henry, M. Willander, E. Janzén, and J-E. Sundgren, Appl. Phys. Lett. **65**, 725 (1994).
23. L. Hultman, M. Shinn, P. B. Mirkarimi, and S. A. Barnett, J. Cryst. Growth **135**, 309 (1994).
24. N. Hirashita, J. E. Greene, U. Helmersson, J. Birch, and J-E. Sundgren, J. Appl. Phys. **70**, 4963 (1991).